Pressure distributions from HENA

(IMAGE meeting, SSL, Berkeley, CA, 2003-03-11)

P. C:son Brandt, D. G. Mitchell, E. C. Roelof, R. Demajistre

March 10, 2003

1 INVERSION STATUS

We use a constrained linear inversion (*Twomey*, 1977; *C:son Brandt et al.*, 2002a; *Demajistre et al.*, 2003) to retrieve the ion distributions from HENA images. It still assumes dipole field. We have focused on obtaining quantitative pressures and refined the way we select the constraint strength. The constraint strength is set by the parameter γ and Figure 1 shows a result with a "bad" and a "good" γ.

2 PRESSURES

Figure 2 shows the proton pressure obtained at 18:00 UT during the 4 October 2000 storm. Here we've used the 10-198 keV range. An eastward rotation of the pressure peak can be seen, but some storms show a peak around midnight and also pre midnight for weaker storms. See *C:son Brandt et al.* (2002b). We are investigating the dependence of the location on IMF and energy. *Fok et al.* (2001) and R. A. Wolf has been able to reproduce this rotation in their models that self-consistently calculates the electric field produced by the closure of the (partial) ring current through the ionosphere.

Figure 3 shows the results of the statistical study by *Ebihara et al.* (2002). They manually selected a couple of hundred main phases of storms (defined as when the Dst decreases) where POLAR was close to the equatorial plane and binned the proton spectra in 6 local time bins. This result is different from previous statistical studies such as *De Michelis et al.* (1999). The earlier studies have not been careful enough in the selection criteria of main phases and therefore also included early recovery phases in their definition of "active" times. The HENA observations are consistent with the results of *Ebihara et al.* (2002).

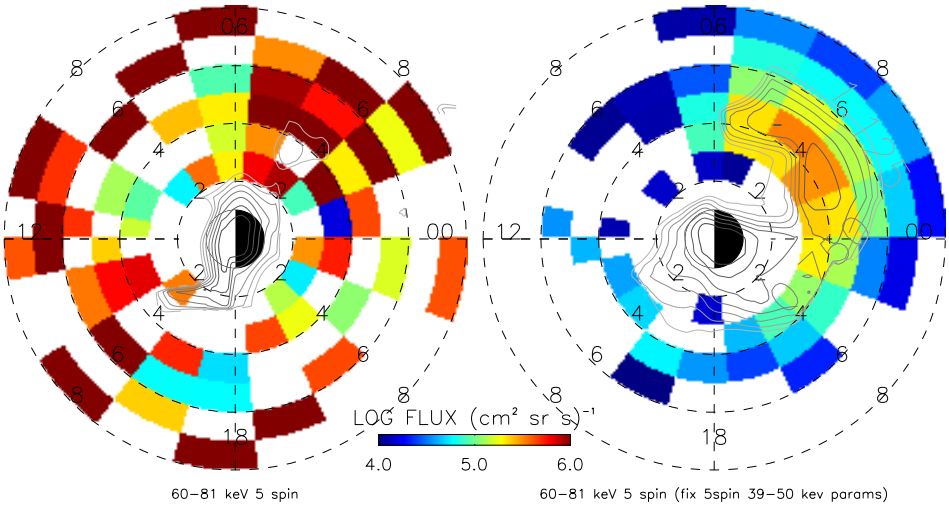

Figure 1: 60-81 keV 10 min integration. (a) Inversion with $\gamma = 3 \times 10^{-32}$. (b) Inversion $\gamma = 1.8 \times 10^{-10}$.

3 CURRENTS AND B-FIELD

Having pressure allows us to compute the 3D current distribution that the pressure drives by using the force balance equation.

$$\mathbf{J} \times \mathbf{B} = \nabla \cdot \mathbf{P} \tag{1}$$

With an isotropic (scalar) pressure P the current can be written

$$\mathbf{J} = \nabla Q \times \nabla P, \tag{2}$$

where the Euler potential Q can be written for a dipole field

$$Q(L, \mu) = \frac{R_E}{B_0} L^4 \mu p(\mu) \tag{3}$$

where $\mu = \cos\theta$ is the cosine of the co-latitude θ; $B_0 = \mu_0 M/(4\pi R_E^3)$, and $p(\mu)$ is a sixth degree polynomial in μ. The components of the current then become

$$J_r = -\frac{L^2}{R_E B_0}\left(\frac{8\mu^2 p(\mu)}{\sin^6\theta} + \sin^2\theta\right)\frac{\partial P}{\partial \phi} \tag{4}$$

$$J_\theta = -\frac{4L^2}{R_E B_0}\frac{\mu p(\mu)}{\sin^5\theta}\frac{\partial P}{\partial \phi} \tag{5}$$

$$J_\phi = \frac{L^3 \sin^3\theta}{R_E B_0}\frac{\partial P}{\partial L} \tag{6}$$

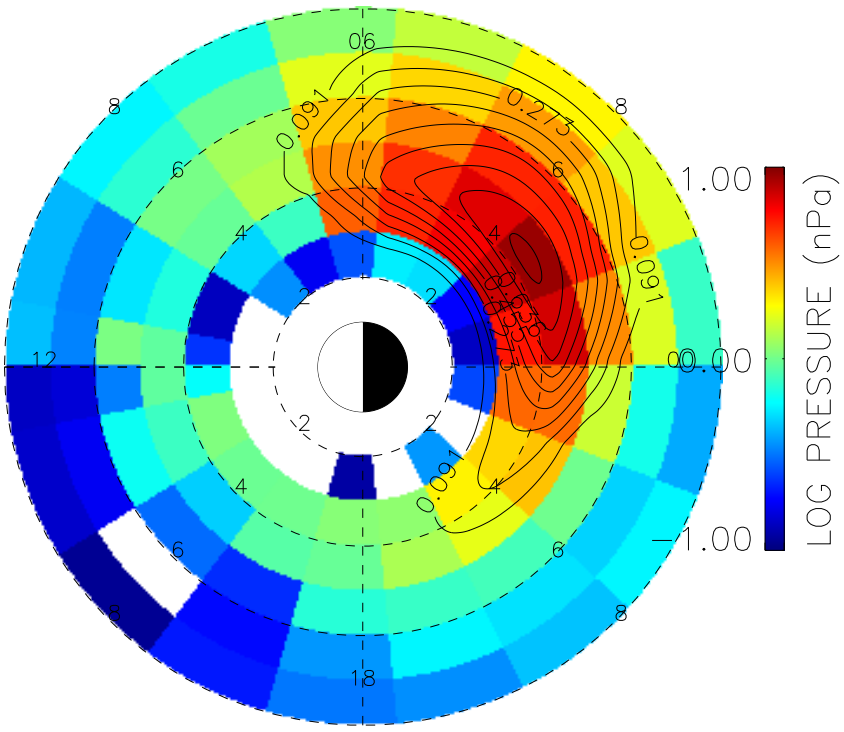

Figure 2: The 10-198 keV proton pressure on 18:00 UT 4 October 2000.

The field-aligned current (FAC) depends only on the azimuthal pressure gradients, while azimuthal current component depends only on the radial pressure gradients. Figure 4 shows the current flow lines computed from the pressure distribution in figure 2.

Once the currents are derived one may compute the magnetic distortion on the geomagnetic field lines by using Bios-Savart's law. A convenient approach can be taken by using Euler potentials and, again, assuming isotropic pressure (which is an oversimplification that we're working on).

$$\Delta\mathbf{B}(\mathbf{r}) = -\mu_0 P(\mathbf{r})\nabla Q(\mathbf{r}) - \int_0^\infty \frac{dR}{R}\int_{4\pi} d^2\Omega P(L',\phi')(3\frac{\mathbf{RR}}{R^2} - \mathbf{I})\cdot\nabla' Q(L',\mu') \tag{7}$$

Figure 5 shows the diamagnetic distortion of a 50 nPa ring current pressure. The dashed lines are the dipole field lines. This is only the distortion caused by the pressure driven system. Thus, one must take into account the region 1 current system that we don't see, to get a better picture of the stretching. At low altitudes the FACs produced by the ring current pressure are very large. However, the region 1 FACs are oppositely directed and equally large, so that

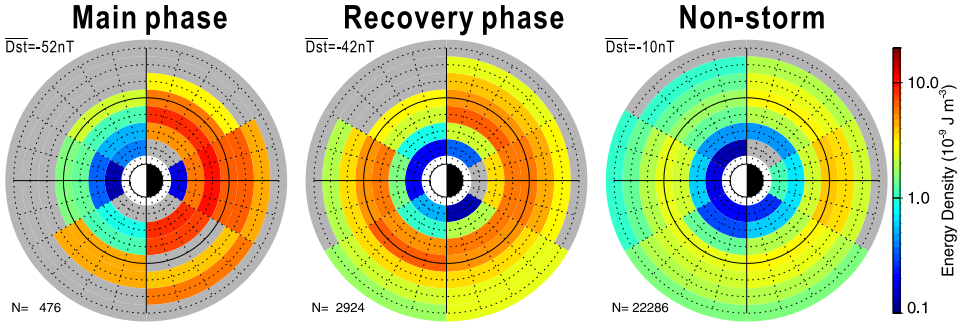

Figure 3: From *Ebihara et al.* (2002). Shows the 1-200 keV proton energy densities (multiply with 2/3 to get pressure in Pa).

the diamgnetic effects from the FACs at low altitudes are smaller than the one we show.

See *Roelof* (2002).

4 IMPROVEMENTS

4.1 Multiple vantage points

The inversion algorithm is generel enough to accept multiple vantage points. It gives the first and second moment of the PADs, j_0 and j_1. We can simplify the interpretation of the pitch angle moments, $\mathbf{J^p_{ion}}$, if only the first two terms are taken ($p = 0, 1$). Considering only the first two moments

$$\begin{aligned} \sum_{p=0}^{2} j_{ion}^{(k)} P_p^*(0) &= j_{ion}^{(0)} - j_{ion}^{(1)} \\ \sum_{p=0}^{2} j_{ion}^{(k)} P_p^*(1) &= j_{ion}^{(0)} + j_{ion}^{(1)} \end{aligned} \tag{8}$$

we can immediately identify the quantities

$$\begin{aligned} j_{ion}^{\perp} &\equiv j_{ion}^{(0)} - j_{ion}^{(1)} \\ j_{ion}^{\parallel} &\equiv j_{ion}^{(0)} + j_{ion}^{(1)} \end{aligned} \tag{9}$$

which are the equatorial ion intensities perpendicular and parallel to the field lines, respectively.

We have preformed tests with vantage points over the pole and at low latitude. We can then obtain a rough estimate on the perpendicular and parallell fluxes. Figure 6 shows an example from the bastille Day storm recovery. During recovery phases the ring current is expected to be stable enough so that we can use two images taken from two different vantage points. We see the isotropic component, the perpendicular and parallell component. The input image consisted of an almost symmetric ring current. The blank areas outside the contours

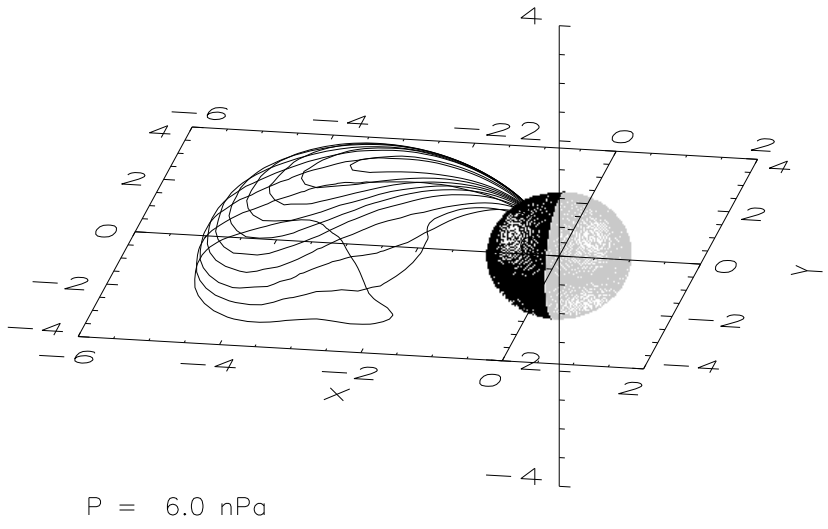

Figure 4: The electric current flow lines in the main phase of the 4 October 2000 storm.

(relative error contours) come from the fact that the Earth is obscuring parts of the ring current at the low-latitude vantage points.

4.2 Pre-specified PADs

In conjcuntion with multiple vantage point inversions, we are working towards integrating in-situ data with the inversion. One can use PADs compiled from statistical datasets from e.g. POLAR/MICS and AMPTE/CCE. As a first example we have taken the PADs compiled by *De Michelis et al.* (1999) and constructed a simple functional representation shown in Figure 7. We see that the PADs are more isotropic on the nightside and more pancake on the dayside, which comes from the fact that smaller pitch angles are "etched" away by the atmospheric interaction as they drift westward around the Earth. The function can then easily be incorporated into the inversion.

From one vantage point there is not enough information in the second PAD component, and we know that the PADs are not isotropic and not the same throughout the equtatorial plane. So there's a need to have the PADs vary in

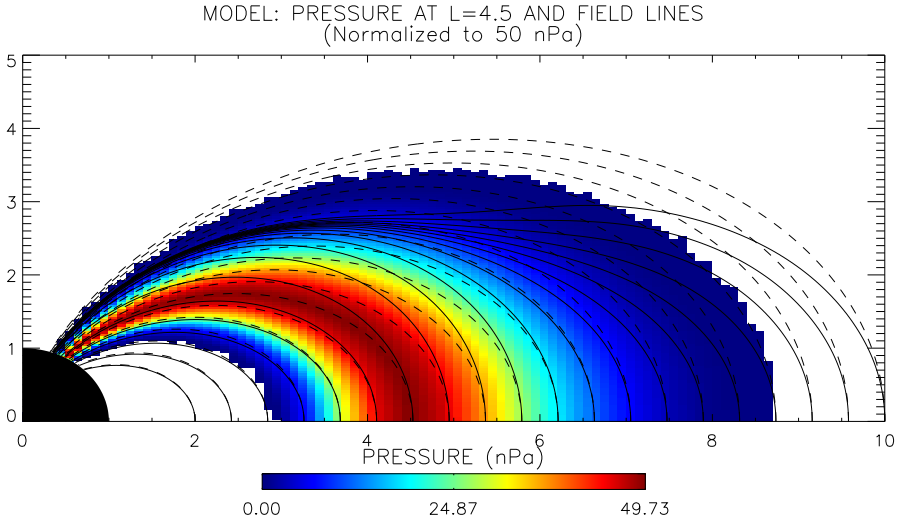

Figure 5: The diamagnetic effect caused by a 50 nPa ring current pressure.

space. The inversion problem is already heavily over determined as it is, so the best way to go is to assimilate in-situ data. Can we "force " the inversion to use an a-priori PAD. Statistical studies have shown that during "active times" the PADs are isotropic around midnight and becomes more peaked around 90° towards noon. See e.g. *De Michelis et al.* (1999).

The problem is if where we should put Expression (17). Currently, the ENA counts are expressed as

$$C_i^{high} = \sum_p \int_0^{2\pi} \int_{R_{atm}}^{\infty} f_i^p(L,\phi,\mu_{eq}) j_{ion}^p(L,\phi) dL d\phi \tag{10}$$

where

$$f_i^p(L,\phi,\mu_{eq}) \equiv \sigma_H^{10} \int_{\theta_1}^{\pi-\theta_1} n^H < A_i > J_0 O P_p^*(\mu_{eq}) d\theta \tag{11}$$

$$j_{ion}(L,\theta,\mu_{eq}) = U(\mu_{eq},\mu_{eqlc}(L),m) \sum_{p=0}^{\lambda} j_{ion}^{(k)} P_p^*(\mu_{eq}) \tag{12}$$

where the functions $P_p^*(\mu_{eq})$ are the Legendre polynomials scaled to the interval $(0,1)$, the parameter m is set to 1 if the loss cone is present or 0 if is not. The function $U(\mu_{eq},\mu_{eqlc}(L),m)$ is a binary function that is zero if $\mu_{eq} > \mu_{eqlc}(L)$ and $m = 1$. The U function therefore governs the behavior of the loss cone, which is considered either completely filled ($m = 0$) or completely empty ($m = 1$).

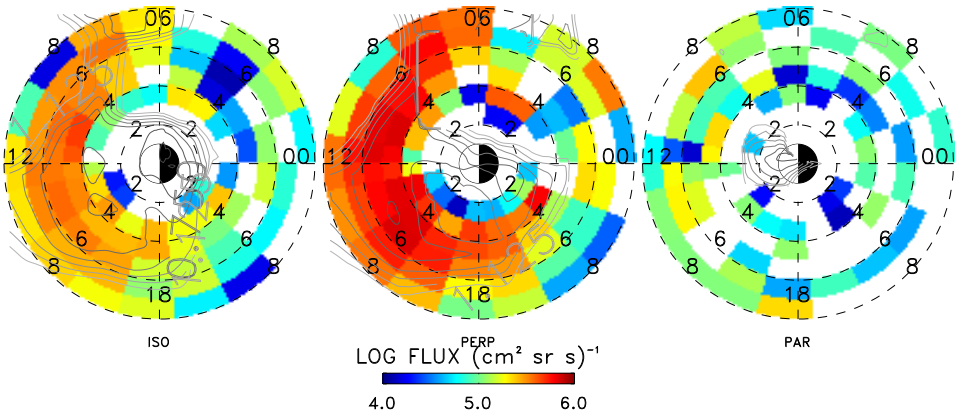

Figure 6: (a) Isotropic component, (b) perpendicular, and (c) parallell.

In order to incorporate the in-situ PAD information we need to reformulate the governing equations in the inversion algorithm. Here we only briefly outline how this can be done. In general the detected ENA counts C_i in pixel i can be written as a volume integral

$$C_i = \int\int\int dL d\theta d\phi \sigma_{10} n_H \langle A_i \rangle \, j_{ION}(L, \phi, \mu_{eq}) \tag{13}$$

where σ_{10} is the charge exchange cross section, n_H is the geocoronal number density, and $\langle A_i \rangle$ is the response function of the instrument. The differential ion intensity, $j_{ION}(L, \phi, \mu_{eq})$, is the general, pitch-angle dependent flux in the equatorial plane. The intensity can always be written

$$j_{ION}(L, \phi, \mu_{eq}) = j_{\perp,ION}(L, \phi) P(L, \phi, \mu_{eq}, \{p_n\}) \tag{14}$$

where $j_{\perp,ION}(L, \phi)$ is the ion intensity at 90° pitch angle and $P(L, \phi, \mu_{eq}, \{p_n\})$ is a function that describes the shape of the PAD and its spatial variation in the equatorial plane by definition P=1 for μ_{eq}=0. Note that this is not the normalized Legendre expansion used by *Demajistre et al.* (2003). The set of p_n is a (small) set of additional parameters needed. This is the function that then needs to be fitted to the in-situ data. A suitable function for this task can be derived from the one used by *Roelof and Skinner* (2000). We start by writing the PAD in one point as

$$P(L, \phi, \mu_{eq}, \{p_n\}) = \exp(-k\mu_{eq}^2) \tag{15}$$

The function k determines the sharpness of the PAD, so that when $k \to 0$ the PAD becomes isotropic. The PAD becomes more pancake like for larger k. In

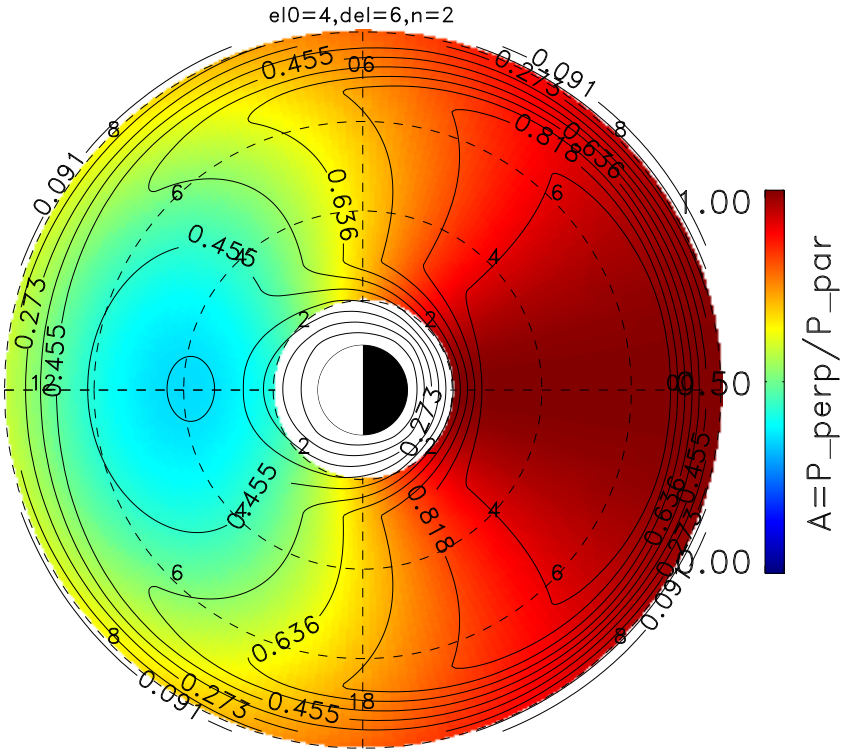

Figure 7: A simple functional representation of the anisotropy compiled by *De Michelis et al.* (1999).

order to model the spatial variation of the PAD, k can be constructed as a function of L and ϕ described by as few as two parameters (p_1, p_2), so that we can write the the equatorial ion distribution in the inversion as

$$j^{eq}_{ION}(L,\phi;p_n) = j^0_{ION}\exp[-k(L,\phi;\{p_n\})\mu^2_{eq}] \tag{16}$$

The function k can be determined by e.g. mimicking the behavior of the results from the AMPTE/CCE CHEM and MEPA dataset (see also *De Michelis et al.* (1999) (their Plate 2)). Strictly speaking, one could obtain an optimum set of parameters p_n by computing a goodness of fit for multiple inversions using different parameters. Although this approach has not yet been tested it is straightforward to implement.

One candidate function for (16) can derived from the following expression, that closely mimics the behavior of the storm-time PADs (*De Michelis et al.*, 1999).

$$A = \frac{P_\perp}{P_\parallel} = 1 - cos(\frac{\phi}{2})\exp[-(\frac{L-L_0}{\Delta L})^n] \tag{17}$$

4.3 Non-dipolar B-field

We will be working towards including a tsyganenko type field model, but to the expense of computational power. It is also possible, in principle, to attempt a self-consistent approach. In that case we can compute the field line distortion in the first step as mentioned above, and then use the resulting field in the next iteration. We feel the representing PAD correctly have higher priority than this. Furthermore, we have not completed the characterization of how the constrained linear inversion dependends on the different parameters and constraint types. The magnetic field enters in how the local pitch cosine is written as a function of equatorial pitch cosine and colatitude.

$$1 - \mu^2 = \frac{B(\theta)}{B(\pi/2)}(1 - \mu_{eq}^2) \tag{18}$$

or exploiting the dipole shape of the magnetic field

$$\mu^2 = 1 - (1 - \mu_{eq}^2)\frac{\sqrt{4 - 3\sin^2\theta}}{sin^6\theta} \tag{19}$$

where $B(\theta)$ is the magnitude of the magnetic field (at constant L) for a given θ.

We have done tests together with M. -C. Fok to see what the effects of using a dipole field is. Fok provided me with an ion distribution from a run of her model in a T96 field; and she also simulated the ENA image in the same T96 field. Then I inverted her ENA image (using a dipole field). We could then compare our inverted ion distribution with her original one. The result is displayed in figure 8.

In a dipole field we have made use of the fact that we can easily relate the L-shell to the spherical coordinates, $L = r/(R_E \sin\theta)$. In a non-dipolar field our problem consists in computing the L-shell for each r, θ, ϕ. Then, for each equatorial L-shell (non-dipolar) compute the volume integral ("the obscuration integral"(?)) that Ed cooked up, if at all possible.

Tsyganenko has developed a fast mapping algorithm based on Euler potentials. Given a point r, θ it computes the r_{eq}, θ_{eq} at the magnetic equator (defined as the point of minimum B on the same field line). One could therefore use T's mapping and map all points in r, θ, ϕ space to the equatorial plane and keep that us a look-up table. This only needs to be done once (for each B-field model). Alternatively compute the L-shells. Might be enough just to do the mapping.

5 HOMEPAGE

Check `sd-www.jhuapl.edu/IMAGE` for publications and meeting notes and interactive data analysis tool.

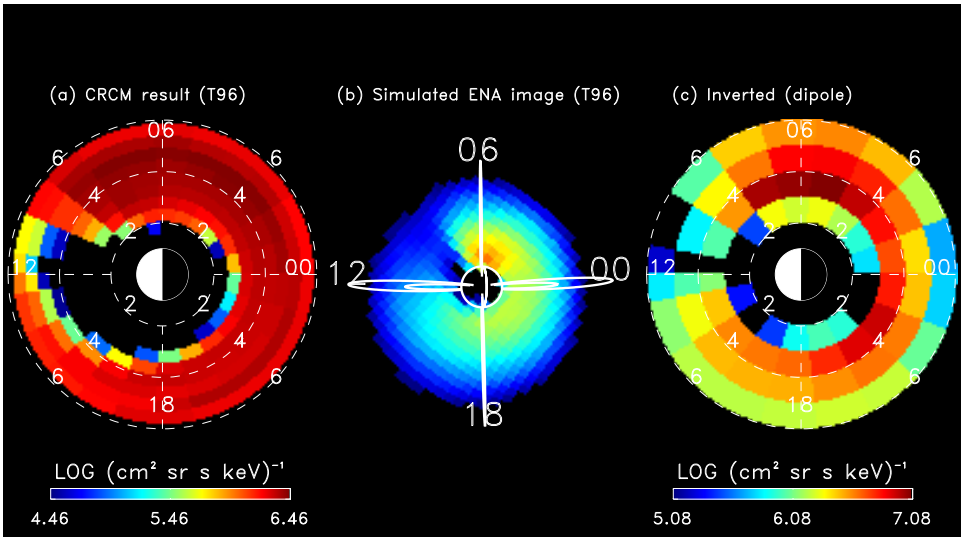

Figure 8: (a) Fok's input ion distribution from a run in a T96 magnetic field. (b) Simulated ENA image using a T96 field. (c) Inversion result using a dipole field. Note the underestimation of radial distance and perhaps of gradients too.

References

C:son Brandt, P., R. Demajistre, E. C. Roelof, D. G. Mitchell, and S. Mende, IMAGE/HENA: Global ENA imaging of the plasmasheet and ring current during substorms, *J. Geophys. Res.*, *107*, SMP 21–1 to SMP 21–13, 2002a.

C:son Brandt, P., S. Ohtani, D. G. Mitchell, M. C. Fok, E. C. Roelof, and R. Demajistre, Global ENA observations of the storm mainphase ring current: Implications for skewed electric fields in the inner magnetosphere, *Geophys. Res. Lett.*, *29*, 15–1 – 15–3, 2002b, 2002GL015160.

De Michelis, P., I. A. Daglis, and G. Consolini, An average image of proton plasma pressure and of current systems in the equatorial plane derived from AMPTE/CCE-CHEM measurements, *J. Geophys. Res.*, *104*, 28,615–28,624, 1999.

Demajistre, R., E. C. Roelof, P. C:son Brandt, and D. G. Mitchell, Retrieval of global magnetospheric ion distributions from high energy neutral atom (ENA) measurements by the IMAGE/HENA instrument, *J. Geophys. Res.*, 2003, to be submitted.

Ebihara, Y., M. Ejiri, H. Nilsson, I. Sandahl, A. Millillo, M. Grande, J. F. Fennell, and J. L. Roeder, Statistical distribution of the storm-time proton ring current: Polar measurements, *Geophys. Res. Lett.*, *29*, 30–1 – 30–4, 2002, 2002GL015430.

Fok, M. C., R. A. Wolf, R. W. Spiro, and T. E. Moore, Comprehensive computational model of Earth's ring current, *J. Geophys. Res.*, *106*, 8417–8424, 2001.

Roelof, E. C., A new approach to extracting energetic ion distributions from ENA images, *J. Geophys. Res.*, 2002, to be submitted.

Roelof, E. C., and A. J. Skinner, Extraction of ion distributions from magnetospheric ENA and EUV images, *Space Sci. Rev.*, *91*, 437–459, 2000.

Twomey, S., *Introduction to the mathematics in remote sensing and indirect measurements*, Developments in geomathematics 3, 1st ed., Elsevier scientific publishing company, 1977.